A new reaction path for the C + NO reaction: dynamics on the $^4A''$ potential-energy surface

Erik Abrahamsson,[a] Stefan Andersson,[a] Nikola Marković[b] and Gunnar Nyman*[a]

Received 4th March 2008, Accepted 12th May 2008
First published as an Advance Article on the web 16th June 2008
DOI: 10.1039/b803787f

We present a new reaction path without significant barriers for the C + NO reaction, forming ground state N(^{4}S) and CO. Electronic structure (CASPT2) calculations have been performed for the two lowest $^4A''$ states of the CNO system. The lowest of these states shows no significant barriers against reaction in the C + NO or O + CN channels. This surface has been fitted to an analytical function using a many-body expansion. Using this surface, and the previously published $^2A'$ and $^2A''$ surfaces [Andersson *et al*., *Phys. Chem. Chem. Phys*., 2000, **2**, 613; Andersson *et al*., *Chem. Phys*., 2000, **259**, 99], we have performed quasiclassical trajectory (QCT) calculations, obtaining rate coefficients for the C(^{3}P) + NO($X^2\Pi$) → CO($X^1\Sigma^+$) + N(^{4}S,^{2}D) and C(^{3}P) + NO($X^2\Pi$) → O(^{3}P) + CN($X^2\Sigma^+$) reactions. We have also simulated the crossed molecular beam experiments of Naulin *et al*. [*Chem. Phys*., 1991, **153**, 519] The inclusion of the $^4A''$ surface in the QCT calculations gives excellent agreement with experiments. This is the first time an adiabatic pathway from C(^{3}P) + NO($X^2\Pi$) to CO($X^1\Sigma^+$) + N(^{4}S) has been reported.

1. Introduction

The reactive system C + NO is of importance for processes as diverse as high-temperature combustion and reactions at low temperatures in interstellar space. The reaction of carbon with nitric oxide is a part of nitrogen reburning, *i.e*. removal of NO and eventual formation of N_2 in combustion processes.[1,2] In the cold and dark inner parts of interstellar molecular clouds, the C + NO reaction is believed to be one of the main sources of the CN radicals that are observed in these regions.[3]

The reactions

$$C(^3P) + NO(X^2\Pi) \rightarrow CN(X^2\Sigma^+) + O(^3P) \qquad (1)$$

and

$$C(^3P) + NO(X^2\Pi) \rightarrow CO(X^1\Sigma^+) + N(^2D) \qquad (2)$$

have so far been the only processes believed to lead to products. This assumption is largely based on calculations performed by Halvick *et al*.[4] in the mid-80s. Their work studied several potential-energy surfaces for the C + NO reaction, and concluded that only the $^2\Pi$ surface, corresponding to $^2A'$ and $^2A''$ surfaces for non-linear configurations, was available for reaction. It was noted at the time that the $^4\Pi$ surface had no barrier in the entrance channel, but a high barrier (about 1 eV) in the strong-interaction region. The possibility of direct reaction on a quartet surface was not considered in that study, only indirectly through spin–orbit coupling to a doublet surface. Due to spin conservation, reaction on the lowest doublet surfaces will only give the excited N(^{2}D) product. To directly form ground-state N(^{4}S), the reaction has to proceed on quartet surfaces. Based on these findings, subsequent studies of the C + NO reaction have only considered reactions (1) and (2).[5–9] Nitrogen has been detected in its ground state experimentally, but it was suggested to be most likely the result of relaxation of N(^{2}D) after the reaction, rather than direct formation of N(^{4}S).[10]

In the 1970s Schmatjko and Wolfrum performed detailed studies of the reaction O(^{3}P) + CN($X^2\Sigma$) → CO($X^1\Sigma^+$) + N(^{4}S,^{2}D), involving both quasiclassical trajectory (QCT) calculations on empirical LEPS-type (London–Eyring–Polanyi–Sato) potential-energy surfaces and experimental investigations of the dynamics and kinetics.[11,12] From their room-temperature experiments they inferred that about 20% of the reactive events produced N(^{4}S). For this to be possible, the reaction somehow has to occur on, or cross over to, a quartet surface. We have recently published dynamics of O + CN → N + CO, concluding that reaction on the $^4\Sigma^-$ surface[13] is not possible for collinear geometries at room temperature.

Breaking the collinear symmetry of a $^4\Sigma^-$ state results in an electronic state of $^4A''$ symmetry. This electronic state allows the reactions

$$O(^3P) + CN(X^2\Sigma^+) \rightarrow CO(X^1\Sigma^+) + N(^4S) \qquad (3)$$

and

$$C(^3P) + NO(X^2\Pi) \rightarrow CO(X^1\Sigma^+) + N(^4S). \qquad (4)$$

If these reaction paths are open at room temperature, the findings of Schmatjko and Wolfrum, as well as the ground-state nitrogen detected in the C + NO experiments, can be explained.

In their *ab initio* study of several doublet and quartet potential-energy surfaces of the CNO system, Yazidi *et al*.[14] showed that the lowest quartet surface is $^4\Pi$ for collinear CNO

[a] *Physical Chemistry, Department of Chemistry, University of Gothenburg, SE-412 96 Gothenburg, Sweden. E-mail: nyman@chem.gu.se*
[b] *Physical Chemistry, Department of Chemical and Biological Engineering, Chalmers University of Technology, SE-412 96 Gothenburg, Sweden*

 This journal is © the Owner Societies 2008

in the C + NO and O + CN channels. For non-linear geometries this surface splits into a $^4A'$ and a $^4A''$ surface, of which the $^4A''$ surface shows a lowering of potential energy upon bending of the CNO complex with a minimum around 120°. For NCO collinear configurations the lowest $^4A''$ surface will correspond to a $^4\Sigma^-$ surface in the N + CO and O + CN channels. In the strong interaction region the $^4\Pi$ and $^4\Sigma^-$ surfaces cross, meaning that the lowest $^4A''$ surface can correlate to several different electronic symmetries at collinear configurations.

In this paper we present an *ab initio* potential-energy surface corresponding to an electronic state of $^4A''$ symmetry. We present an analytical fit of the surface, using a many-body expansion. The fitted surface has been used to perform quasiclassical trajectory calculations for the C + NO reaction, corresponding to reaction (4) above. We have also performed new QCT calculations using the previously published $^2A'$ and $^2A''$ surfaces, corresponding to reactions (1) and (2). From these calculations we obtain thermal rate coefficients, reaction cross sections and product energy distributions. The article continues by giving the details about the calculations in section 2. In section 3 the results are presented and compared to experiments and the findings are discussed. Finally, our main conclusions are summarized in section 4.

2. Computational details

2.1 *Ab initio* calculations

A total of 4947 *ab initio* points have been calculated with multi-state CASSCF/CASPT2 (complete active space second-order perturbation theory), using the g_1 Fock matrix and an ANO-L basis set with the 14s9p4d3f primitive set contracted to 5s4p3d2f and the MOLCAS 6.0 program package.[15] Scalar relativistic effects were included in the one-electron integrals with the relativistic no-pair Douglas–Kroll transformation. To ensure convergence to the correct states, the CASSCF calculations were performed with state-averaging with equal weights for both states of $^4A''$ symmetry. The active space was the full valence space except the 2s electrons on the oxygen atom, giving 13 active electrons in 11 active orbitals.

The geometries were chosen with 15 values in the Jacobi coordinate R, *i.e.* the distance from the atom to the centre of mass of the diatomic molecule, in the range 1.5 to 9.0 Å. The bond length r of the three diatomic fragments was given by eight values in the range 0.90 to 1.30 Å. The angle θ between the $\boldsymbol{R}$ and $\boldsymbol{r}$ vectors was given by nine values from 0 to 180°. Additional *ab initio* points for collinear configurations were calculated with inter-atomic distances between 1.3 and 1.7 Å, as well as triangular configurations with inter-atomic distances in the range 1.0 to 1.5 Å and angles between the inter-atomic axes in the range 40 to 170°. The *ab initio* points fall in the energy range [−11.05, 2.00] eV.

2.2 Analytic fit

The *ab initio* points have been fitted to an analytic expression using a many-body expansion. The potential-energy surface is described as a sum of two- and three-body interactions:

$$V(R_1, R_2, R_3) = \sum_{i=1}^{3} V^{(2)}(R_i) + V^{(3)}(R_1, R_2, R_3), \quad (5)$$

where R_i are the three inter-atomic distances.

The two-body terms, $V^{(2)}$, are the diatomic potentials for CN, NO and CO of the extended Rydberg type with added dispersion interaction:

$$V^{(2)}(R) = V_{\mathrm{Ry}} + V_{\mathrm{dc}}, \quad (6)$$

which have been fitted to *ab initio* data. The extended Rydberg potential, V_{Ry}, is given by the expression[16]

$$V_{\mathrm{Ry}} = -D_{\mathrm{e}}(1 + a_1\rho + a_2\rho^2 + a_3\rho^3)\exp(-\gamma\rho), \quad (7)$$

$$\gamma = \gamma_0[1 + \gamma_1\tanh(\gamma_2\rho)], \quad (8)$$

$$\rho = R - R_{\mathrm{e}}, \quad (9)$$

where R is the inter-atomic distance and D_{e}, a_1, a_2, a_3, γ_0, γ_1, γ_2 and R_{e} are fit parameters. D_{e} and R_{e} are similar to the well depth and the equilibrium distance, respectively, but they are not fixed to the values of these quantities. At long range the dynamic correlation corresponds to the dispersion interaction, and for a diatomic molecule Varandas[17] has suggested the form

$$V_{\mathrm{dc}} = -\sum_{n=6,8,10} C_n\chi_n(R)R^{-n}, \quad (10)$$

where χ_n is a damping function:

$$\chi_n(R) = \left[1 - \exp\left(-A_n\frac{R}{\rho} - B_n\frac{R^2}{\rho^2}\right)\right]^n, \quad (11)$$

$$A_n = \alpha_0 n^{-\alpha_1}, \quad (12)$$

$$B_n = \beta_0\exp(-\beta_1 n), \quad (13)$$

$$\rho = 5.5\ \mathrm{Bohr} + 1.25R_0 \quad (14)$$

with $\alpha_0 = 16.36606$, $\alpha_1 = 0.70172$, $\beta_0 = 17.19338$ and $\beta_1 = 0.09574$ being universal dimensionless parameters for all isotropic interactions.[18] R_0 is the Le Roy radius defined as:

$$R_0 = 2(\langle r_{\mathrm{A}}^2\rangle^{1/2} + \langle r_{\mathrm{B}}^2\rangle^{1/2}) \quad (15)$$

with $\langle r_{\mathrm{X}}^2\rangle$ being the expectation value of the squared radii of the outermost electron in atom X.[19]

The three-body term, $V^{(3)}$, is expressed as an Mth-order polynomial of the form developed by Aguado and Paniagua:[20]

$$V^{(3)}(R_1, R_2, R_3) = \sum_{i,j,k}^{M} d_{ijk}S_1^i S_2^j S_3^k \quad (16)$$

with the additional constraints

$$i + j + k \neq i \neq j \neq k, \quad (17)$$

$$i + j + k \leq M. \quad (18)$$

The polynomial variables are of the form used by Stark and Werner:[21]

$$S_n = R_n\exp[-\kappa_n(R_n - R_n^0)], \quad (19)$$

where R_n^0 and κ_n are parameters. The polynomials are constructed such that they vanish when $R_n = 0$ and $R_n \to \infty$. In this work we have used $M = 10$, resulting in 255 linear parameters d_{ijk}.

To optimize the six non-linear and 255 linear parameters, the fit to the *ab initio* energy points was performed using a self-consistent method, where the non-linear parameters are optimized using a quadratic minimization of the root-mean-square (RMS) deviation from the *ab initio* energy points and those calculated using the analytical expression described above. For every cycle of the quadratic minimization of the non-linear parameters, the optimal set of linear parameters are determined using standard techniques for the determination of the minimal least-squares solution of an overdefined system. This is the same procedure as used in our previous studies of the $^2A''$ and $^2A'$ surfaces.[7,8]

2.3 Trajectory calculations

The quasiclassical trajectory calculations (QCT) were carried out using the same trajectory program as in our previous 3D and 2D studies.[7–9,13] We have performed calculations for the C + NO reaction at different temperatures, as well as for conditions corresponding to crossed molecular beam experiments.[22] In the former case, thermal rate coefficients have been calculated; in the latter, reaction cross sections and product energy distributions, in the same manner as in ref. 8.

In our trajectory calculations, a complex is considered to have formed if at least one minimum distance exchange occurs, *i.e.* if the shortest distance between any two nuclei does not involve the same pair of nuclei at all times. The complex is defined to live from the first internuclear minimum distance exchange until the last.

2.4 Electronic degeneracy factors

Following the discussion in our previous work,[9] we introduce electronic degeneracy factors for the different electronic surfaces. The general expression for the electronic degeneracy factors is given by

$$f(T) = \frac{Q_{A-BC}(T)}{Q_A(T)Q_{BC}(T)} \tag{20}$$

where $Q_A(T)$ and $Q_{BC}(T)$ are reactant electronic partition functions, and $Q_{A-BC}(T)$ is the partition function of the reactant fine structure states that adiabatically correlate with the surfaces leading to reaction. Assuming that the surfaces at hand are the only ones available for reaction, the rate coefficients obtained from the quasi-classical trajectory calculations are multiplied by the appropriate degeneracy factor, and summed to give the total rate coefficient.

The previously calculated $^2A'$ and $^2A''$ surfaces each correspond to two electronic states, which results in electronic degeneracy factors given by the form

$$f_{^2A}^{C+NO} = \frac{1+\exp(-23.6/T)}{[1+3\exp(-23.6/T)+5\exp(-62.4/T)][2+2\exp(-172.4/T)]} \tag{21}$$

for each of the two surfaces, as previously described. The assumption is that the two states of each doublet surface correlate to the lowest asymptotic fine-structure states, *i.e.* $C(^3P_0)$ + $NO(X^2\Pi)$ and $C(^3P_1)$ + $NO(X^2\Pi)$. Note that eqn (8) in ref. 9 was multiplied with a factor 2 compared to eqn (21). In our previous work, each of the two $^2A'$ and $^2A''$ surfaces were compared to experiments separately, which accounts for the doubling of the electronic degeneracy factor in that work.

The $^4A''$ surface has four states leading to reaction, and the electronic degeneracy factor is given by

$$f_{^4A}^{C+NO} = \frac{4\exp(-23.6/T)}{[1+3\exp(-23.6/T)+5\exp(-62.4/T)][2+2\exp(-172.4/T)]}, \tag{22}$$

assuming that the $^4A''$ states all correlate to the $C(^3P_1)$ + $NO(X^2\Pi)$ reactant state. This is based on a "building-up" principle where the next higher potential-energy surface correlates to the next higher asymptotic fine-structure state.

The quantities obtained from the crossed molecular beam simulations have to be weighted by both the cross sections for the surface in question, and by normalized fine-structure state populations $w(J)$. The fine-structure state population depends on the electronic temperature of the beams, which in this case is an unknown quantity, and an educated guess of the distribution has to be made. Naulin *et al.*[22] observed that less than 5% of the NO molecules were in the upper $\Omega = 3/2$ fine-structure state in the experiments. Assuming that *all* NO is in the lower $\Omega = 1/2$ state, simple weight functions can be derived as follows. The $^2A'$ and $^2A''$ surfaces both correlate asymptotically to a $C(^3P_0)$ + $NO(X^2\Pi_{1/2})$ and a $C(^3P_1)$ + $NO(X^2\Pi_{1/2})$ state, meaning that the $J = 0$ and one of the three $J = 1$ fine-structure states react through the doublet surfaces. The $^4A''$ surface correlates to four $C(^3P_1)$ + $NO(X^2\Pi_{1/2})$ states, *i.e.* the remaining two $J = 1$ fine-structure states react through the $^4A''$ surface. Each of the $C(^3P_J)$ fine structure states is multiplied by the two states of the $NO(X^2\Pi_{1/2})$ molecule, giving in total two states for $C(^3P_0)$ + $NO(X^2\Pi_{1/2})$ and six for $C(^3P_1)$ + $NO(X^2\Pi_{1/2})$. Thus, the "raw" cross sections for each of the three surfaces should be weighted with a factor given by

$$\sigma_{^2A'} = \left[\frac{w(J=0)}{2} + \frac{w(J=1)}{6}\right]\sigma_{^2A'}^{(raw)}, \tag{23}$$

$$\sigma_{^2A} = \left[\frac{w(J=0)}{2} + \frac{w(J=1)}{6}\right]\sigma_{^2A}^{(raw)} \tag{24}$$

and

$$\sigma_{^4A} = \frac{4w(J=1)}{6}\sigma_{^4A}^{(raw)}, \tag{25}$$

where $w(J)$ are the fine-structure state populations.

We have assumed a beam in the high-temperature limit, where an equal distribution over all fine-structure populations is obtained. This gives $w(J = 0) = 1/9$ and $w(J = 1) = 3/9$, since there are 9 fine-structure states in total for $C(^3P_J)$. Thus

 This journal is © the Owner Societies 2008

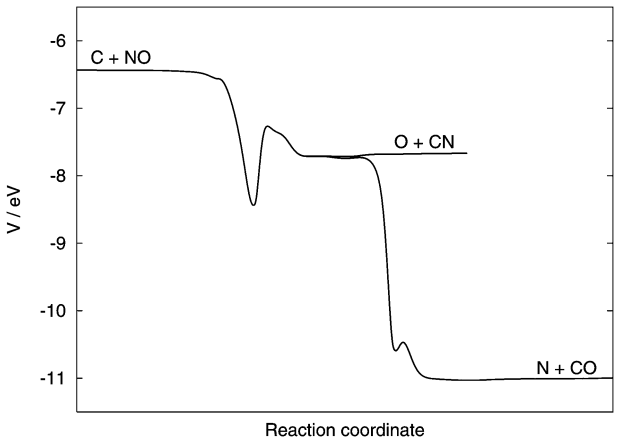

Fig. 1 Minimum energy paths connecting the reactants (C + NO) with the two sets of products (O + CN and N + CO). The energies are relative to separated atoms.

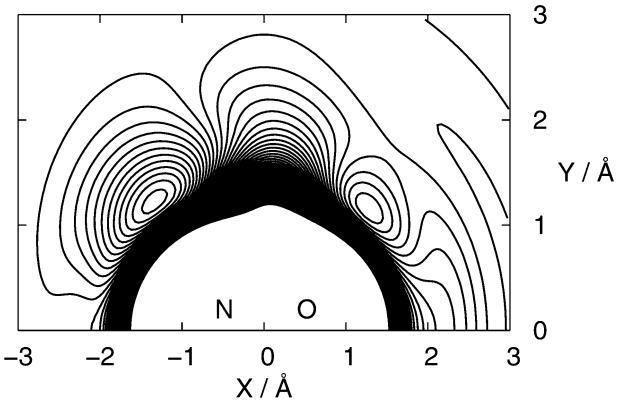

Fig. 2 Polar contour plot of the fitted potential-energy surface for the C + NO channel; r_{NO} = 1.1556 Å. The contours begin at −8.25 eV, end at −4 eV and have a spacing of 0.15 eV. The energies are relative to separated atoms. 45° is at the upper right-hand corner and 135° is at the upper left-hand corner.

we have $\sigma_{^2A'} = 2/18\ \sigma^{(raw)}_{^2A'}$, $\sigma_{^2A''} = 2/18\ \sigma^{(raw)}_{^2A''}$ and $\sigma_{^4A''} = 4/18\ \sigma^{(raw)}_{^4A''}$, from eqn (23)–(25).

The scaling factor g_i for each of the three surfaces will be of the form

$$g_i = \frac{\sigma_i}{\sum_j \sigma_j}, \qquad (26)$$

where σ_i and σ_j come from the respective expressions in eqn (23)–(25).

3. Results and discussion

3.1 Potential-energy surface

The state-averaged CASPT2 calculations produce two potential-energy surfaces of $^4A''$ symmetry. Both surfaces are degenerate in the C + NO and O + CN entrance channels. The two surfaces are, however, of very different character, as only the lower surface results in ground-state carbon monoxide in the N + CO channel. The upper surface results in CO in the excited $a^3\Pi_r$ state, which lies 6.04 eV above the CO ground state.[14,23] Thus, this state is also well above the C + NO entrance channel. It also has barriers against reaction, and is not accessible under thermal conditions. In this work, we have only considered the lower state.

The minimum-energy paths connecting the reactants with the products on the fitted potential-energy surface for the lowest $^4A''$ state are shown in Fig. 1. The corresponding figure for the $^2A''$ surface is shown in ref. 7 (the corresponding figure for the $^2A'$ surface would be similar to the one for $^2A''$ but would lack the triangular CNO minimum[8]). As seen in Fig. 1, the fitted potential-energy surface does not show any significant barriers to forming N + CO from either the C + NO or O + CN arrangement channels. Furthermore, there are no significant barriers against the formation of O + CN from C + NO. Compared to the previously calculated $^2A''$ and $^2A'$ surfaces,[7,8] the reaction path of the $^4A''$ surface goes through fewer local minima and saddle points to form N + CO, and it does not include a global minimum. A summary of the significant stationary points for the $^4A''$ fitted potential-energy surface is presented in Table 1.

In Fig. 2 is shown a polar contour plot of the analytic fit to the C + NO entrance channel for the lower, reactive, $^4A''$ state. NO is kept at its fitted minimum, 1.1556 Å, which also is close to its experimental equilibrium value, 1.151 Å.[23] As seen, there is a deep potential well at 140° approach from the oxygen side of NO, which is entered without barriers, corresponding to the local triangular CNO minimum seen at −8.4 eV in Fig. 1.

Table 1 Significant local minima on the analytical fit of the potential-energy surface[a]

	R_{CN}	R_{NO}	R_{CO}	E	ω_1	ω_2	ω_3	ω_4
Triangular minima								
CNO	2.256	1.208	1.405	−8.435	1530	1096	681	
NCO	1.438	2.305	1.205	−10.59	1713	859	567	
Linear van der Waals complexes								
C–ON	3.676	1.149	2.527	−6.620	2101	262	25	25
O–CN	1.175	4.132	2.957	−7.718	2051	70	73	73
N–OC	4.053	2.924	1.129	−11.05	2136	136	59	59
Product channels								
C + NO		1.156		−6.435	1868			
O + CN	1.178			−7.666	2041			
N + CO			1.134	−11.01	2133			

[a] All distances are in Å, all energies are relative to separated atoms and are quoted in eV, and all frequencies are in cm^{-1}.

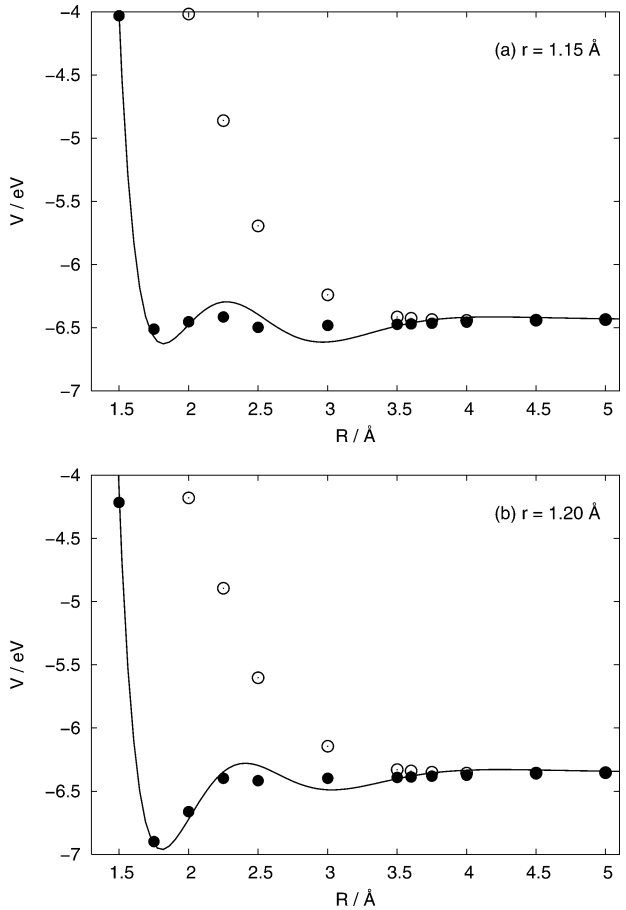

Fig. 3 *R* profile for the C + NO entrance channel at (a) $r = 1.15$ Å and (b) $r = 1.20$ Å, $\theta = 30°$. The lines represent the fitted potential-energy surface. The filled symbols represent the *ab initio* data for the lower state, the unfilled symbols the upper state.

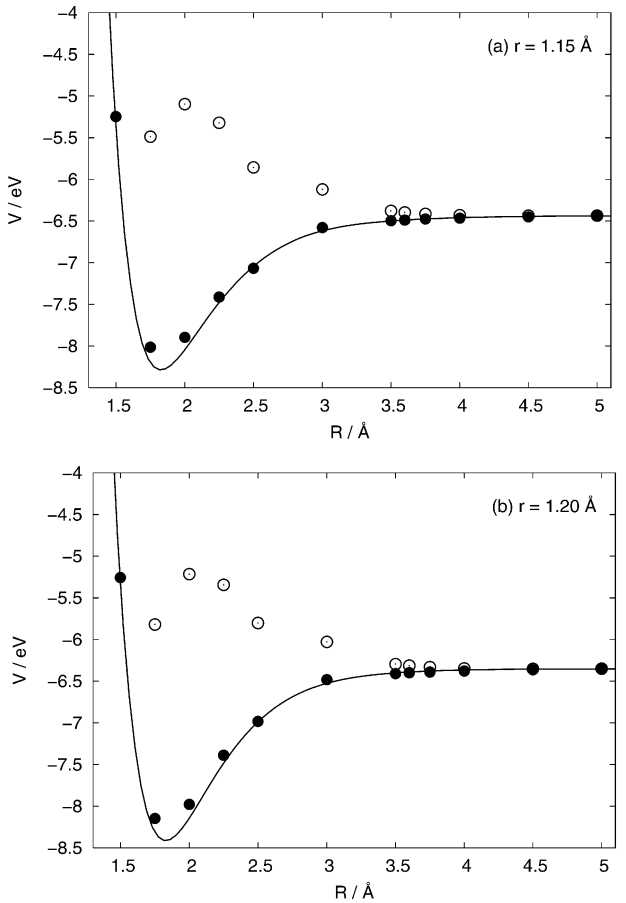

Fig. 4 *R* profile for the C + NO entrance channel at (a) $r = 1.15$ Å and (b) $r = 1.20$ Å, $\theta = 140°$. The lines represent the fitted potential-energy surface. The filled symbols represent the *ab initio* data for the lower state, the unfilled symbols the upper state.

Fig. 2 also shows a slight well at 30 to 55°. Here the fit shows barriers against entering the well, which are not as accentuated in the *ab initio* data (*cf*. Fig. 3). At collinear configurations, the surface has high barriers against reaction, as shown in our previous study.[13] Fig. 3 shows the *ab initio* data and the fitted potential for the C + NO entrance channel, where the NO distance is set at 1.15 and 1.20 Å and the Jacobi angle is 30°. The *ab initio* data for the upper state (unfilled symbols) are included for comparison. It is seen that the *ab initio* data for the lower state only have a slight potential barrier before entering the well, while the fit shows an oscillatory behaviour, with a barrier of 0.13 eV in the case of $r = 1.15$ Å. In the case of the much deeper well at 140°, shown in Fig. 4, the fit to the *ab initio* points is clearly more accurate.

Fig. 5 shows a polar contour of the lower state O + CN entrance channel. The CN distance is kept at its fitted minimum, 1.178 Å, which is close to the experimental equilibrium value of 1.172 Å.[23] This channel also has a potential well around 140° approach from the nitrogen side of CN, as well as a slight well between 30 and 55°. As shown in Fig. 6 and 7, both these wells are entered without apparent barriers.

The RMS deviation between the *ab initio* points and the fit is 0.13 eV, with the maximum deviation being 0.97 eV. For energies less than −5.5 eV, which is the thermally accessible region, the RMS deviation is 0.094 eV. Compared to the previous fits of the doublet surfaces,[7,8] the present fit has about twice as large an RMS deviation. In this work we have calculated state averaged CASPT2 energies for excited states of the CNO system, which makes the convergence of the

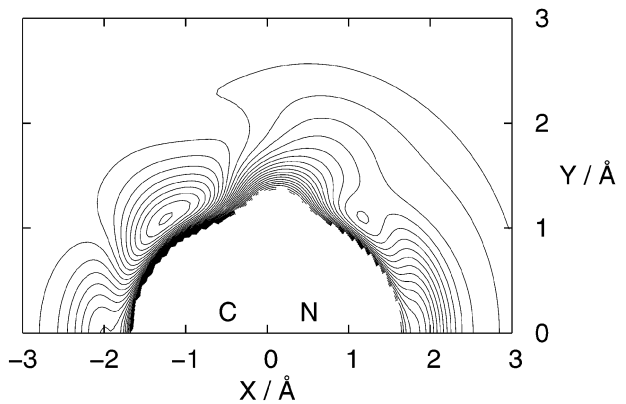

Fig. 5 Polar contour plot of the fitted potential-energy surface for the O + CN channel; $r_{CN} = 1.178$ Å. The contours begin at −9.4 eV, end at −4 eV and have a spacing of 0.15 eV. The energies are relative to separated atoms. 45° is at the upper right-hand corner and 135° is at the upper left-hand corner.

This journal is © the Owner Societies 2008

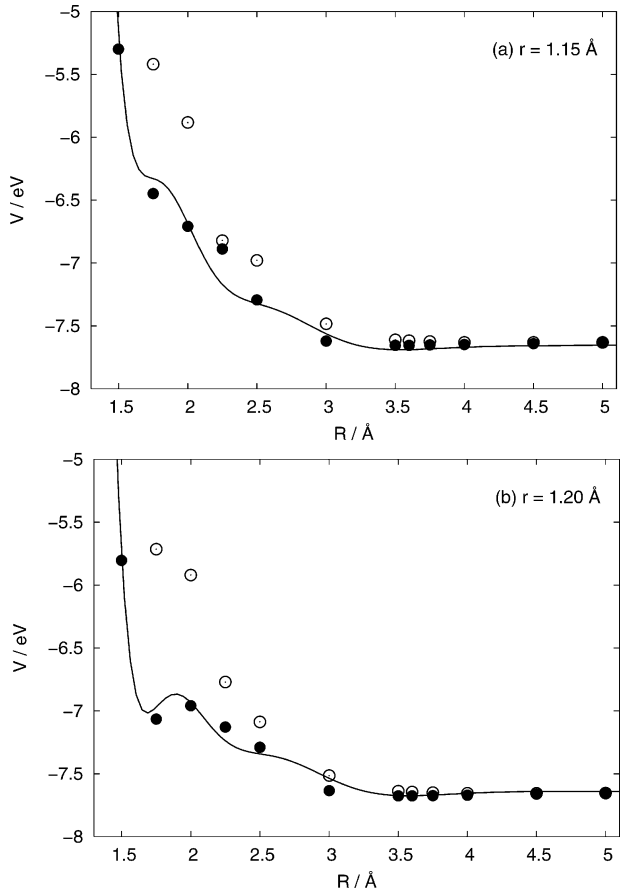

Fig. 6 *R* profile for the O + CN entrance channel at (a) $r = 1.15$ Å and (b) $r = 1.20$ Å, $\theta = 30°$. The lines represent the fitted potential-energy surface. The filled symbols represent the *ab initio* data for the lower state, the unfilled symbols the upper state.

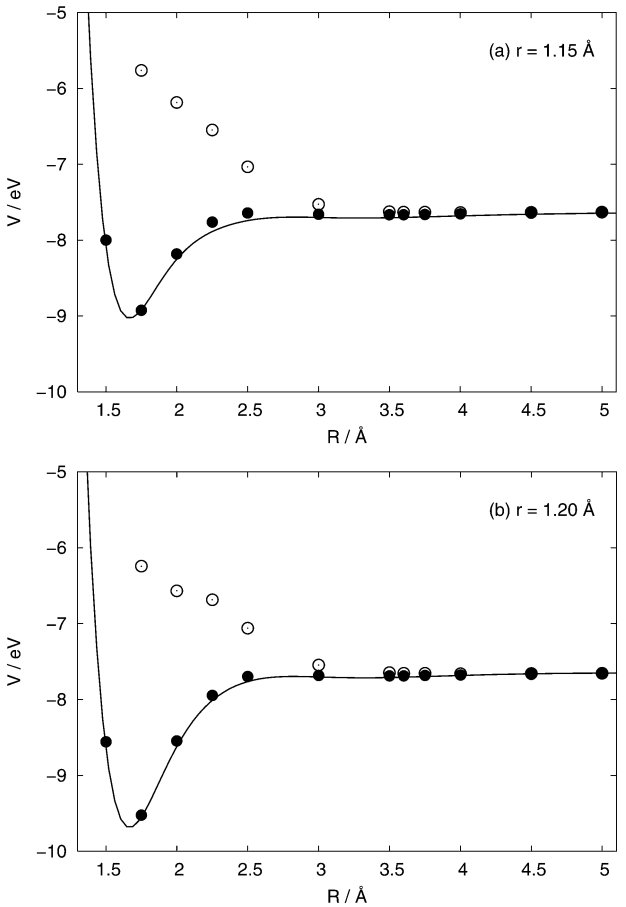

Fig. 7 *R* profile for the O + CN entrance channel at (a) $r = 1.15$ Å and (b) $r = 1.20$ Å, $\theta = 140°$. The lines represent the fitted potential-energy surface. The filled symbols represent the *ab initio* data for the lower state, the unfilled symbols the upper state.

CASPT2 calculations more problematic. The O + CN configuration was found to be particularly sensitive to variations in the fitting parameters and we therefore only consider the reaction from the C + NO entrance channel.

The lower state in the $^4A''$ symmetry asymptotically correlates to N(^{4}S) and CO($X^1\Sigma^+$). Fig. 8 shows a polar contour plot of this surface with $r_{CO} = 1.134$ Å, which is close to its experimental value 1.128 Å.[23] The surface is repulsive at all angles of approach.

These results show that there are previously undiscovered reaction paths without significant barriers from both the C(^{3}P) + NO($X^2\Pi$) and O(^{3}P) + CN($X^2\Sigma^+$) entrance channels to the N(^{4}S) + CO($X^1\Sigma^+$) channel. There is also a previously unreported reaction path without significant barriers from the C(^{3}P) + NO($X^2\Pi$) channel to the O(^{3}P) + CN($X^2\Sigma^+$) channel.

3.2 Thermal rate coefficients

We have performed quasiclassical trajectory calculations for ten temperatures in the range 10–4000 K for the C + NO reaction on the $^4A''$ surface. For each of the ten temperatures, 50 000 trajectories have been run. The rate coefficients for formation of the two products [O(^{3}P) + CN($X^2\Sigma^+$) and N(^{4}S) + CO($X^1\Sigma^+$)] and the total rate coefficient are presented in Fig. 9. The total $^4A''$ rate coefficient has similar temperature dependence to the ones for the $^2A'$ and $^2A''$ surfaces.[9] The rate coefficient for O + CN formation peaks at a low temperature (25 K) and then falls off with increasing temperature, while the rate of formation of N + CO is relatively low at low temperatures and then increases steadily with increasing temperature with a fairly sharp increase above 1000 K. The peak value of the total rate coefficient is about half of those found for the $^2A'$ and $^2A''$ surfaces, reflecting the restricted geometries through which reaction can proceed on the $^4A''$ surface.

Fig. 10 shows the total rate coefficient for the C + NO reaction proceeding on the three surfaces $^2A'$, $^2A''$, and $^4A''$, where the rate coefficient for each surface is weighted with the relevant electronic degeneracy factor from eqn (21) or (22). It is seen that our calculations give excellent agreement with experiments at temperatures above 1000 K[24] and between 50 K and 300 K.[25] At temperatures below 50 K, the calculated rate coefficients are somewhat higher than the experimental values,[25] but still at most by a factor of 1.7.

The experimental branching fractions show no or only weak temperature dependence in the range 295–3790 K, as shown in Fig. 11. Our calculations underestimate the experimental branching fractions somewhat, and they show a seemingly stronger temperature dependence than the available

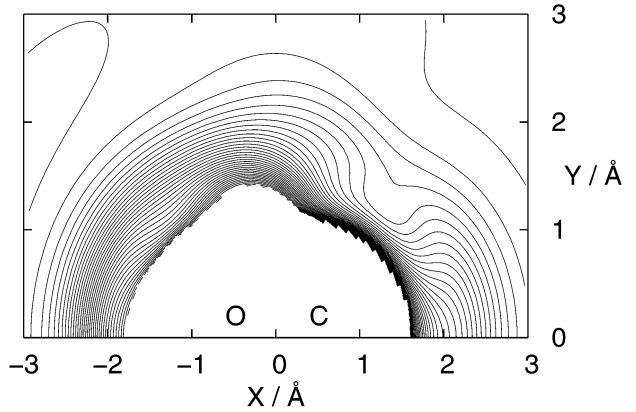

Fig. 8 Polar contour plot of the fitted potential-energy surface for the N + CO channel; r_{CO} = 1.134 Å. The contours begin at −11 eV, end at −4 eV and have a spacing of 0.15 eV. The energies are relative to separated atoms. 45° is at the upper right-hand corner and 135° is at the upper left-hand corner.

experimental data. N(^{4}S) was observed to be formed in the experimental study on this reaction by Bergeat *et al.*,[10] but they questioned whether this was due to direct formation of N(^{4}S) or due to collisional electronic relaxation of N(^{2}D). At room temperature they observed about twice as much N(^{2}D) as N(^{4}S). From our calculations we find this ratio to be about 3. This indicates that a large fraction of the N(^{4}S) observed in these experiments was formed directly. Thus, we have here for the first time shown that it is plausible to form ground-state N(^{4}S) directly from the C(^{3}P) + NO($X^2\Pi$) reaction.

It should be noted that the total rate coefficients in Fig. 10, as well as the branching fractions in Fig. 11, are calculated as though the three surfaces are separated. As discussed in our previous paper,[9] the CNO system exhibits the Renner–Teller effect,[26] which couples the doublet surfaces. There should also be spin–orbit couplings between the ^{4}A″ and the doublet surfaces. Thus, the system might undergo transitions between the surfaces, which would affect the rate coefficients.

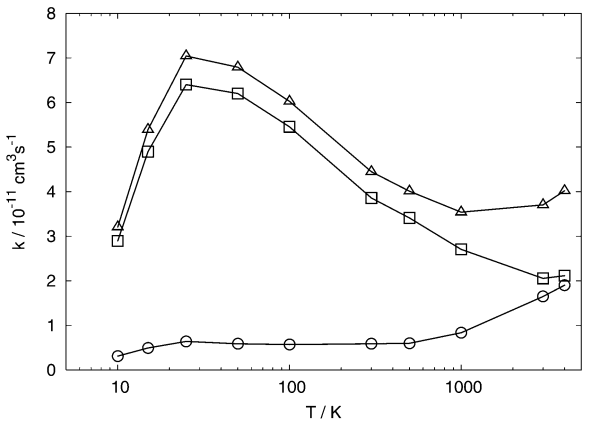

Fig. 9 Thermal rate coefficients for the C + NO reaction on the ^{4}A″ surface; triangles denoting total rate coefficients; squares rate coefficients for formation of O + CN; and circles rate coefficients for formation of N + CO. The results are converged to within the size of the symbols.

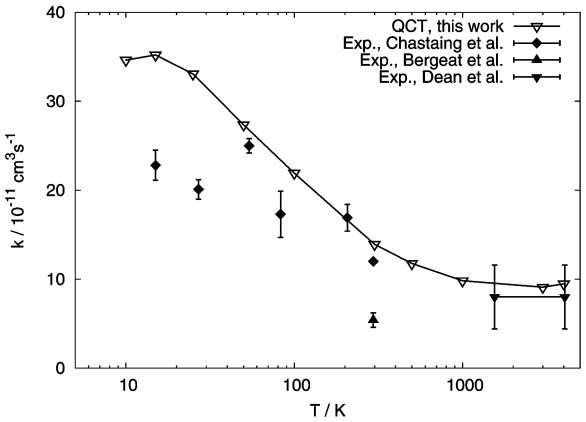

Fig. 10 Total thermal rate coefficients for the C + NO reaction. The open triangles denote the weighted sum of the calculated rate coefficients for the ^{2}A′, ^{2}A″, and ^{4}A″ surfaces, and filled symbols denote experimental results (Bergeat *et al.*,[10] Dean *et al.*[24] and Chastaing *et al.*[25]).

In our previous work[9] it was found that the ^{2}A″ surface gave branching fractions in close agreement with the experimental results, while the ^{2}A′ surface gave a much lower formation of N + CO. The experimentally observed branching fractions were accounted for by a simple approach where all complex-forming trajectories on the ^{2}A′ surface make the transition to the ^{2}A″ surface, under the assumption that the Renner–Teller effect couples these surfaces sufficiently strongly. The approach used in our previous work changes the rate coefficient by factors between 0.8 and 1.1. In the current work we have chosen not to include this effect. The new results from the ^{4}A″ surface increase the branching fractions and bring them much closer to the experimental values at high temperatures (see Fig. 11). This means that the Renner–Teller induced ^{2}A′ → ^{2}A″ transition need not have unit probability for the QCT calculations to match the experimental results. Recently,

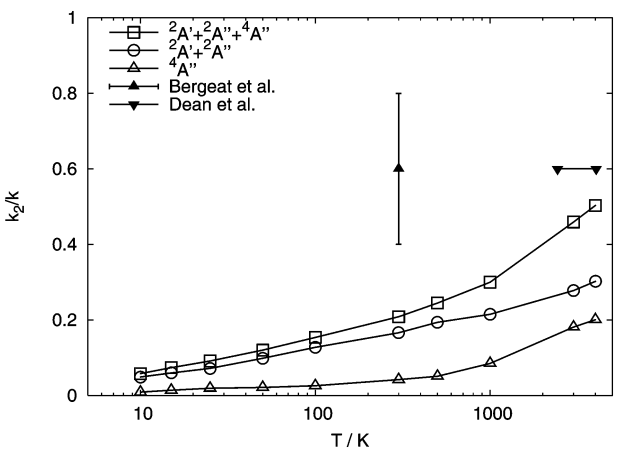

Fig. 11 Branching fractions for the C + NO reaction. k is the total thermal rate coefficient for the C + NO reaction and k_2 the rate coefficient for N + CO formation. Open symbols denote calculated branching fractions for the total formation of nitrogen (squares), formation of excited nitrogen (circles) and formation of ground-state nitrogen (triangles). Filled symbols denote experimental results (Bergeat *et al.*[10] and Dean *et al.*[24]).

This journal is © the Owner Societies 2008

Table 2 Energy distribution for the O + CN products[a]

Results	$\langle\varepsilon_{rot}'\rangle$	$\langle f_{rot}\rangle$	$\langle\varepsilon_{vib}'\rangle$	$\langle f_{vib}\rangle$	$\langle\varepsilon_{tr}'\rangle$	$\langle f_{tr}\rangle$	σ_1	b_{max}	τ
ε_{tr} = 0.06 eV									
Experiment	0.20	0.15	0.40	0.30	0.74	0.55	—	—	—
Present work									
$^2A'$	0.11	0.09	0.62	0.49	0.55	0.43	54.0	6.48	0.12
$^2A''$	0.13	0.10	0.54	0.42	0.62	0.48	53.3	6.21	0.13
$^4A''$	0.29	0.22	0.28	0.22	0.72	0.56	35.7	4.91	0.38
Averaged	0.19	0.15	0.46	0.36	0.64	0.49	19.8	—	0.23
ε_{tr} = 0.23 eV									
Experiment	0.30	0.20	0.45	0.29	0.77	0.51	—	—	—
Present work									
$^2A'$	0.20	0.14	0.61	0.42	0.65	0.45	17.8	4.25	0.16
$^2A''$	0.26	0.18	0.58	0.40	0.62	0.43	15.4	4.03	0.16
$^4A''$	0.33	0.23	0.24	0.17	0.88	0.61	12.5	3.98	0.41
Averaged	0.27	0.19	0.43	0.30	0.75	0.51	6.47	—	0.27

[a] All energies are given in eV. $\langle\varepsilon_i'\rangle$ is the mean amount of energy deposited in the various degrees of freedom: i = rot for rotation, i = vib for vibration, i = tr for translation; $\langle f_i\rangle$ is the fraction of the total energy deposited in these degrees of freedom; σ_1 is the reaction cross-section in Å^2; b_{max} is the maximum impact parameter in Å for O + CN formation, and τ is the complex lifetime in ps of trajectories forming O + CN. Experimental values from Naulin *et al.*[22] The "Averaged" values represent weighted sums of the results for the $^2A'$, $^2A''$ and $^4A''$ surfaces.

both the spin–orbit interactions and Renner–Teller parameters have been calculated for the CNO, NCO and CON complexes.[14,27] Making a detailed investigation of the Renner–Teller effect with, for example, trajectory surface hopping, would be of great interest.

3.3 Crossed molecular beam simulations

We have performed quasiclassical trajectory calculations on the new $^4A''$ surface, as well as on the two doublet surfaces, to model the C + NO crossed molecular beam (CMB) experiments by Naulin *et al.*[22] The calculations were performed in the same manner as in our previous work,[8] and a total of 100 000 trajectories were run at each of the two energies studied.

The results from the CMB simulations on the $^4A''$ surface are compared with the experimental product energy distributions[22] in Table 2, together with the combined results from all three surfaces, weighted according to eqn (26). It is clear from Table 2 that the addition of the $^4A''$ surface to the previous calculations gives much better agreement with the experimental data than with only the doublet surfaces taken into account. For the case of ε_{tr} = 0.23 eV the agreement with experiments is excellent. For the lower energy the deviations are somewhat larger, but the agreement between experiments and calculations is still very good.

The good agreement between the calculated and experimental results is further illustrated in Fig. 12 and 13, where vibrational distributions of the CN products are displayed. In Fig. 12(a) and 13(a) the vibrational distributions of the individual surfaces are shown for the two cases ε_{tr} = 0.06 eV and ε_{tr} = 0.23 eV respectively. The distribution for the $^4A''$ surface is closer to a statistical distribution (*cf.* Fig. 7 and 8 in ref. 22) than for the doublet surfaces, which indicates long-lived complexes. This is reflected in the long average lifetimes τ on the $^4A''$ surface, which are around three times longer than those for the doublet surfaces. An explanation for these different behaviours is that almost all trajectories enter the well of the triangular CNO complex on the $^4A''$ surface, compared to only 9% entering the deep linear NCO minimum on the $^2A'$ and 19% on the $^2A''$ surface.[8] On the doublet

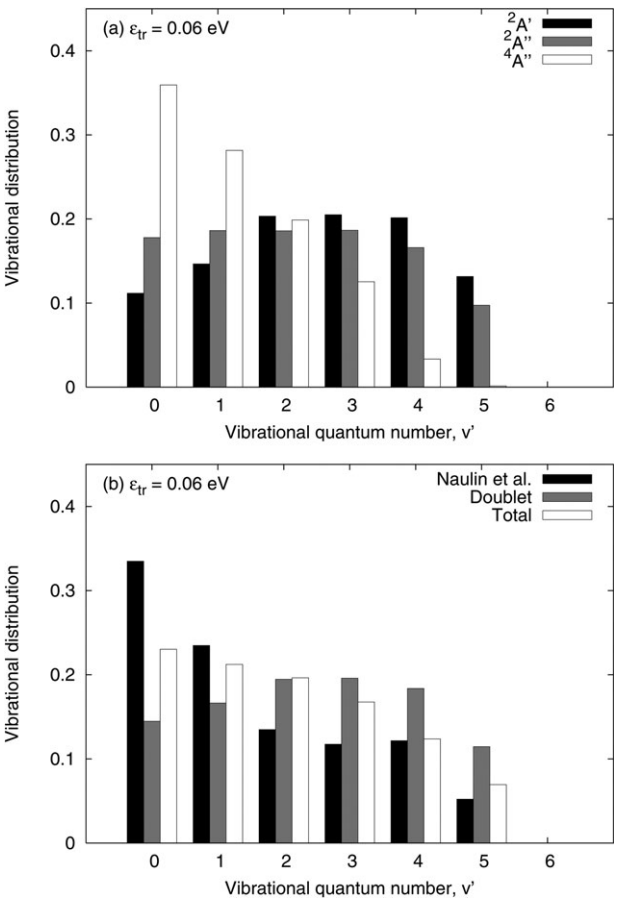

Fig. 12 Distribution of vibrational quantum numbers, v', in the CN products. The bars correspond in (a) to calculated distributions on the $^2A'$, $^2A''$ and $^4A''$ surfaces, and in (b) to the total vibrational quantum number distribution from Naulin *et al.*,[22] the weighted sum of the vibrational distributions on the two doublet surfaces, and the weighted sum of the vibrational distributions on all three surfaces. ε_{tr} = 0.06 eV.

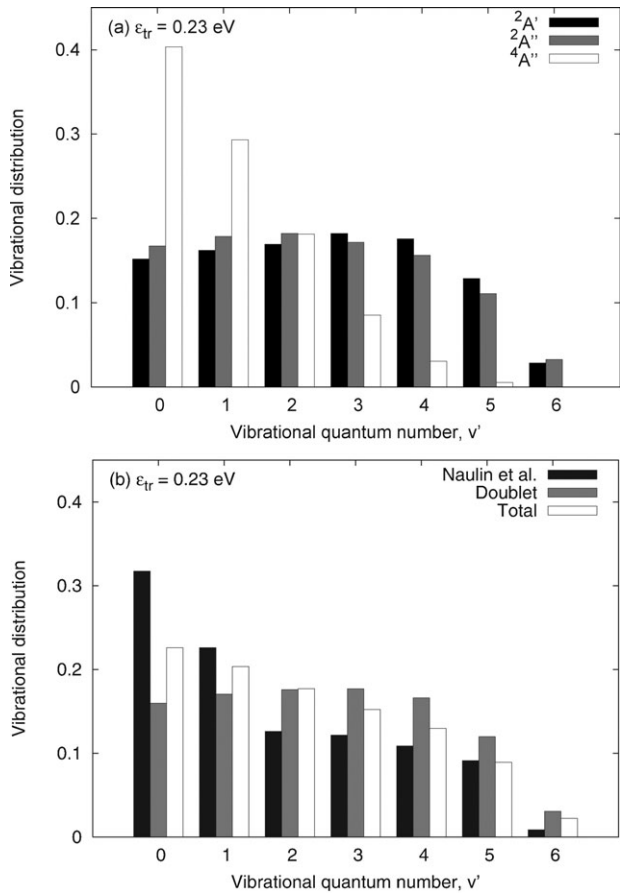

Fig. 13 Distribution of vibrational quantum numbers, v', in the CN products. The bars correspond in (a) to calculated distributions on the $^2A'$, $^2A''$ and $^4A''$ surfaces, and in (b) to the total vibrational quantum number distribution from Naulin *et al.*,[22] the weighted sum of the vibrational distributions on the two doublet surfaces, and the weighted sum of the vibrational distributions on all three surfaces. ε_{tr} = 0.23 eV.

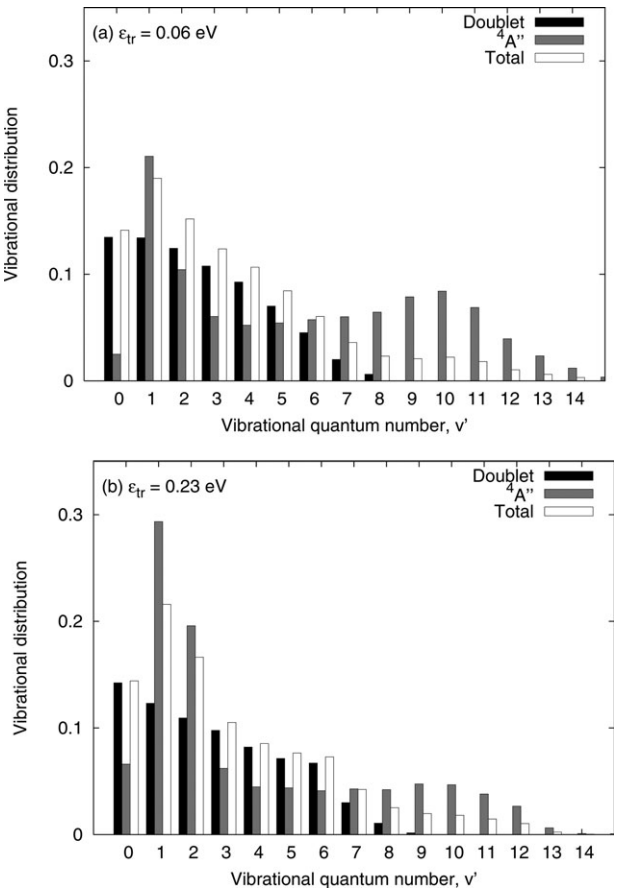

Fig. 14 Distribution of vibrational quantum numbers, v', in the CO products for ε_{tr} = 0.06 eV (a) and ε_{tr} = 0.23 eV (b). The bars correspond to the weighted sum of the calculated distributions on the two doublet surfaces, the calculated distributions on the quartet surface, and the weighted sum of all three surfaces.

surfaces the C + NO → CN + O reaction otherwise proceeds quite rapidly through the linear CNO minimum.

By making a weighted linear combination of the vibrational distributions of CN obtained from the $^4A''$ surface with the results from the doublet surfaces we obtain a much closer agreement with experiments, as shown in Fig. 12(b) and 13(b), where the experimental results are compared to our previous calculations[8] and the present work. The contribution from the $^4A''$ surface increases the total fraction in the lower vibrational states and decreases the fraction in the higher vibrational states. For all vibrational states, except $v' = 2$, the inclusion of the $^4A''$ surface improves the agreement with experiments compared to the results on the doublet surfaces.

In Table 3, the energy distribution and cross-sections are given for the N + CO products. Noticeable is the great difference in complex lifetimes on the $^4A''$ surface for the two translational energies. While the complex life time at ε_{tr} = 0.06 eV is of the same order as for the $^2A''$ surface, the reaction is virtually instant (20 fs) at ε_{tr} = 0.23 eV. Fig. 14

Table 3 Energy distribution for the N + CO products[a]

Results	$\langle\varepsilon_{rot}'\rangle$	$\langle f_{rot}\rangle$	$\langle\varepsilon_{vib}'\rangle$	$\langle f_{vib}\rangle$	$\langle\varepsilon_{tr}'\rangle$	$\langle f_{tr}\rangle$	σ_2	b_{max}	τ
ε_{tr} = 0.06 eV									
$^2A'$	0.53	0.25	0.67	0.32	0.89	0.43	1.67	5.97	0.73
$^2A''$	0.43	0.20	0.66	0.32	1.00	0.48	19.1	5.89	0.23
$^4A''$	0.78	0.17	1.42	0.31	2.42	0.52	3.73	4.86	0.19
Total	0.53	0.19	0.86	0.31	1.37	0.50	3.13	—	0.25
ε_{tr} = 0.23 eV									
$^2A'$	0.57	0.25	0.79	0.34	0.91	0.40	1.56	4.06	0.53
$^2A''$	0.55	0.25	0.70	0.31	1.01	0.44	12.5	3.88	0.19
$^4A''$	0.72	0.15	0.98	0.21	3.09	0.64	4.41	3.75	0.02
Total	0.62	0.19	0.82	0.25	1.80	0.56	2.54	—	0.15

[a] Notations used are as in Table 2.

This journal is © the Owner Societies 2008

shows the vibrational distributions of the CO product. The doublet surfaces show a more statistical distribution of vibrational states than the $^4A''$ surface, which gives a distribution with two peaks: one at $v' = 1$ and one at $v' = 9$–10. The total distribution with all three surfaces taken into account show a pronounced peak at $v' = 1$ and a plateau around $v' = 10$.

4. Conclusions

Ab initio calculations using CASPT2 have been performed for the CNO system in the $^4A''$ symmetry. We have presented a new analytical potential-energy surface fitted to the *ab initio* energy points using a many-body expansion.

Thermal rate coefficients have been obtained for the C + NO reaction using quasiclassical trajectory calculations on the $^4A''$ surface and the previously published $^2A'$ and $^2A''$ surfaces. These new calculations give somewhat larger rate coefficients for the whole temperature range than those with only the doublet surfaces included. Nevertheless, the newly obtained rate coefficients are still in very good agreement with experimental values. At temperatures below 50 K the new rate coefficients are somewhat larger than the ones obtained experimentally.

We have performed quasiclassical trajectory calculations simulating crossed molecular beam experiments, calculating reaction cross sections and product energy distributions for all three surfaces. The agreement with the experimental distribution of vibrational quantum numbers in CN is significantly improved with the inclusion of the $^4A''$ surface. The energy distributions among the system degrees of freedom in the O + CN products show excellent agreement with experiments. Thus, with the inclusion of the $^4A''$ surface in the calculations, some of the previous deviations from experimental results can be explained.

These results show that ground-state nitrogen can be formed from the reaction of carbon and nitric oxide at temperatures accessible in interstellar clouds and in combustion processes. The results furthermore indicate that there should be a reaction path going from ground-state O + CN to ground-state CO + N.

Acknowledgements

The computations were performed on Chalmers Centre for Computational Science and Engineering (C3SE) computing resources. The staff at C3SE is acknowledged for their assistance concerning technical aspects. Support from the Swedish Research Council is gratefully acknowledged. This study is supported in part by the European Community's Human Potential Programme under contract MCRTN 512302, Molecular Universe.

References

1. P. Glarborg, M. U. Alzueta, K. Dam-Johansen and J. A. Miller, *Combust. Flame*, 1998, **115**, 1.
2. C. Schulz, H.-R. Volpp and J. Wolfrum, in *Chemical Dynamics in Extreme Environments*, ed. R. A. Dressler, World Scientific, Singapore, 2001, p. 206.
3. G. I. Boger and A. Sternberg, *Astrophys. J.*, 2005, **632**, 302.
4. P. Halvick, J. C. Rayez and E. M. Evleth, *J. Chem. Phys.*, 1984, **81**, 728.
5. B. J. Persson, B. O. Roos and M. Simonson, *Chem. Phys. Lett.*, 1995, **234**, 382.
6. M. Simonson, N. Marković, S. Nordholm and B. Persson, *Chem. Phys.*, 1995, **200**, 141.
7. S. Andersson, N. Marković and G. Nyman, *Phys. Chem. Chem. Phys.*, 2000, **2**, 613.
8. S. Andersson, N. Marković and G. Nyman, *Chem. Phys.*, 2000, **259**, 99.
9. S. Andersson, N. Marković and G. Nyman, *J. Phys. Chem. A*, 2003, **107**, 5439.
10. A. Bergeat, T. Calvo, G. Dorthe and J. C. Loison, *Chem. Phys. Lett.*, 1999, **308**, 7.
11. K. J. Schmatjko and J. Wolfrum, *Ber. Bunsen-Ges. Phys. Chem.*, 1975, **79**, 696.
12. K. J. Schmatjko and J. Wolfrum, *Ber. Bunsen-Ges. Phys. Chem.*, 1978, **82**, 419.
13. E. Abrahamsson, S. Andersson, G. Nyman and N. Marković, *Chem. Phys.*, 2006, **324**, 507.
14. O. Yazidi, H. Gritli and G. Chambaud, *Mol. Phys.*, 2005, **103**, 3321.
15. G. Karlström, R. Lindh, P.-Å Malmqvist, B. O. Roos, U. Ryde, V. Veryazov, P.-O. Widmark, M. Cossi, B. Schimmelpfennig, P. Neograd y and L. Seijo, *Comput. Mater. Sci.*, 2003, **28**, 222.
16. A. J. C. Varandas and J. D. da Silva, *J. Chem. Soc., Faraday Trans.*, 1992, **88**, 941.
17. A. J. C. Varandas, *Mol. Phys.*, 1987, **60**, 527.
18. A. J. C. Varandas, *J. Chem. Phys.*, 1997, **106**, 9647.
19. R. J. Le Roy, in *Molecular Spectroscopy*, ed. R. F. Barrow, D. A. Long and D. J. Millen, Chemical Society of London, London, 1973, vol. 1.
20. A. Aguado and M. Paniagua, *J. Chem. Phys.*, 1992, **96**, 1265.
21. K. Stark and H.-J. Werner, *J. Chem. Phys.*, 1996, **104**, 6515.
22. C. Naulin, M. Costes and G. Dorthe, *Chem. Phys.*, 1991, **153**, 519.
23. K. P. Huber and G. Herzberg, in *NIST Chemistry WebBook, NIST Standard Reference Database, Number 69*, ed. P Linstrom and W Mallard, National Institute of Standards and Technology, Gaithersburg, MD, 2005 (http://webbook.nist.gov).
24. A. J. Dean, R. K. Hanson and C. T. Bowman, *J. Phys. Chem.*, 1991, **95**, 3180.
25. D. Chastaing, S. D. Le Picard and I. R. Sims, *J. Chem. Phys.*, 2000, **112**, 8466.
26. G. Herzberg, *Molecular Spectra and Molecular Structure, III. Electronic Spectra of Polyatomic Molecules*, Van Norstrand, Princeton, NJ, 1966.
27. C. Léonard, H. Gritli and G. Chambaud, *J. Mol. Spectrosc.*, 2007, **243**, 90.